



Analysis of a Jet Pump Performance under Different Primary Nozzle Positions and Inlet Pressures using two Approaches: One Dimensional Analytical Model and Three Dimensional CFD Simulations

William Orozco Murillo^{1,2}, José Alfredo Palacio-Fernandez^{2,3}, Iván David Patiño Arcila^{2,4}, Johan Steven Zapata Monsalve^{2,5}, John Alexander Hincapié Isaza^{2,6}

¹ Grupo de Investigación e Innovación Ambiental GIAM, Po. Box, 050034 Medellín, Colombia, Email: William.ozco@pascualbravo.edu.co

² Facultad de Ingeniería, Institución Universitaria Pascual Bravo, Calle 73 # 73A – 226. 050034 Medellín, Colombia

³ Grupo de Investigación e Innovación Ambiental GIAM, Po. Box, 050034 Medellín, Colombia, Email: josealpa@pascualbravo.edu.co

⁴ Grupo de Investigación e Innovación Ambiental GIAM, Po. Box, 050034 Medellín, Colombia, Email: i.patinoar@pascualbravo.edu.co

⁵ Semillero de Investigación Ambiental SIA, Po. Box, 050034 Medellín, Colombia, Email: johansz.13@hotmail.com

⁶ Semillero de Investigación Ambiental SIA, Po. Box, 050034 Medellín, Colombia, Email: jhonhincapie11@gmail.com

Received April 12 2020; Revised August 13 2020; Accepted for publication August 14 2020.

Corresponding author: J.A. Palacio-Fernandez (josealpa@pascualbravo.edu.co)

© 2020 Published by Shahid Chamran University of Ahvaz

Abstract: A jet pump operates under the Venturi effect, where a fluid enters through a primary nozzle and, when passing through a convergent-divergent nozzle, it reaches supersonic conditions, originating a vacuum pressure in a secondary fluid. Fluid-dynamics simulations of jet pumps are performed here using standard $k-\epsilon$ turbulence model. Numerical results are compared to those obtained with an analytical model previously developed, concluding that both approaches predict a similar behavior of Mach number, fluid pressure and fluid velocity. A parametric study is done to determine the influence of inlet pressure and primary nozzle position in jet pump performance, Mach number field and total pressure profile. Both parameters have an important influence in those variables, but this is not monotonic in all cases.

Keywords: Computational Fluid Dynamics, Analytical flow modeling, Inlet pressure, Primary nozzle position, Jet pump performance.

1. Introduction

A jet pump is a type of pump that operates under the principle of a high-pressure fluid jet and the Venturi effect that is generated in it. Some advantages of jet pumps are simplicity of construction, high reliability, low cost and wide range of operating conditions. The Venturi effect occurs when a fluid passes through a convergent-divergent nozzle, undergoing subsonic and supersonic conditions. In jet pumps, the motive or primary fluid enters the nozzle at high pressure and low speed, and, when arrives to convergent part of the nozzle, it accelerates, increasing velocity and reducing pressure; this in turns generates a suction or vacuum in another fluid originally at rest. The geometry, basic operation and main parts of a jet pump are illustrated in (Fig.1a), where the behavior of the fluid pressure and speed along the jet pump is observed. According to [1,2], when the motive fluid reaches sonic velocity at the nozzle throat (P1), a supersonic speed is achieved at the nozzle outlet (P2), as long as the ratio of areas is suitable; this leads to an important pressure drop and therefore, to a high drag coefficient, w . It is important to mention that w is defined as the ratio between the mass flow rate of the secondary fluid and the mass flow rate of the primary one. The mixing process in a jet pump is not simple, as experimentally verified by an optical method [3]. This method allowed precise visualization of two high-speed flows inside the jet pump, by associating Rayleigh scattering, laser induced fluorescence and image processing. Recently, using computational fluid dynamics (CFD), processes of dragging and mixing of fluids in jet pumps were analyzed, concluding that the position of nozzle outlet affects the critical back pressure and the drag ratio [4]. Geometrical parameters are critical for an appropriate design of jet pumps. In this sense, several authors [5,6] have carried out CFD simulations changing the geometry of the primary nozzle in order to study its influence in the drag coefficient, w , obtaining some geometries where w exceeds 0.5. On the other hand, CFD simulations were conducted in [7] for the transport of solid particles in a jet pump, using the Lagrangian-Eulerian approach; these authors used different flow densities and obtained the mass flow rate of solid particles at the pump outlet, as well as the maximum fluid flow velocity, which was found three times less than the motive fluid velocity. Additionally, it was proposed a methodology that predicts the conditions of pressure drooping of the motive fluid, for both over-expanded and under-expanded fluid flow conditions [8]. Several fluid dynamics simulations were performed using CFD software [8], concluding that regulation of the driving pressure and controlled modifications in the nozzle throat can prevent the onset of a blockage condition in the jet pump.

One of the most important applications of the jet pump is the cooling systems; therefore, a lot of work has been focused on this



issue. For example, ANSYS FLUENT™ was used to simulate the flow in a variable-area ejector and compare its operating efficiency with a conventional constant-area ejector, concluding that the pressure-rise ratio increased up to 40% [9]. On the other hand, the performance of a jet pump for refrigeration, in terms of the diffuser throat and diffuser divergent lengths, was analyzed by means of ANSYS Fluent™ in [10], obtaining optimal values for these lengths of 0.3376 m and 0.844 m, respectively, for a vacuum gauge pressure of -100.288 kPa. Other authors [11] presented a model of a jet pump to determine the design area ratio (defined as the ratio of the area of constant section of the suction chamber to the area of the nozzle throat) that optimizes the jet pump performance in a refrigeration system. Moreover, an experimental study about the influence of the primary nozzle geometry on the performance of the jet pump in R141b ejector refrigerators was conducted by [12]. Other authors have found that the change in the length of the constant section of the diffuser influences the performance of the jet pump. For example, some authors [13] found that, even though this change in length does not significantly influence the drag coefficient, it affects the back pressure of the mixture, causing its increase. Considering that the jet pump efficiency significantly depends on its geometry, some researches have conducted parametric studies about this aspect. For example, some authors [14] performed geometrical optimizations of a jet pump by means of CFD software, achieving an improvement in pump performance from 29% to 33%, with a consequent reduction in energy consumption of 20%. The $k-\varepsilon$ turbulence model was used in that work. That model is suitable for fluid flow simulations in jet pumps because is able to predict parameters of overall pump performance, such as the drag coefficient and pressure-rise ratios. Similarly, the influence of some transient phenomena on the jet pump performance using the $k-\varepsilon$ model was studied in [15], finding that eddy flows arising in the secondary fluid near the wall can cause the reduction of the drag coefficient. Using four different turbulence models ($k-\varepsilon$ standard, $k-\varepsilon$ realizable, RSM and SST), CFD simulations were conducted in ANSYS Fluent™ [16] in order to determine how the scaling increase and reduction affects the energy efficiency of the pump, finding a maximum efficiency of 38.46% for an optimum design area ratio of 4.61. Similarly to the present work, the influence of several geometrical parameters (jet pump area ratio, nozzle position and length of mixing chamber) on the jet pump performance was studied in [16]; the parameter to assess the pump performance in that work was the energy efficiency, as defined by the multiplication of the mass flow ratio and pressure ratio, whereas, in the present work, three output parameters are considered: drag coefficient (w), ratio between inlet and nozzle throat pressure (P_p/P_g), and nozzle throat velocity (V_g). This three-parameter based analysis allows discriminating several phenomena involved in the jet pump performance, as shown later.

ANSYS Fluent™ was used by [17] to study the influence of scaling and size of roughness on the jet pump performance, finding that energy efficiency considerably increases up to a determined scale size when absolute roughness is constant, whereas it can be considered independent of scaling at constant relative roughness. Differently to the present work, the transition $k-\omega$ STT model was selected in the referred work [17] on the basis of preliminary experimental tests of a full-scale water pump. Up-scaling and down-scaling of the jet pump were implemented by the authors, but, contrarily to the present work, the relative positions between the parts comprising the jet pump was kept constant in all cases. On the other hand, a numerical two-phase analysis of a jet pump with saturated steam was performed in [18] using the eulerian two-phase model of ANSYS Fluent™ and a direct-contact condensation model. Two parameters were considered to account for the pump performance: mass ratio (drag coefficient), which is considered in the present work as well, and suction lift, defined as the theoretical depth from which the pump is able to suck the fluid under certain operating condition. Input parameters in that work were the primary nozzle pressure and suction nozzle pressure, finding an increase of the mass ratio and a decrease of the suction lift when increasing both input parameters. A unique geometry was considered in that work [18] and numerical results were validated with experiments in a real-scale prototype. In the present work, primary pressure is considered as an input parameter as well, but the suction nozzle pressure is fixed at a certain value to allow the ethanol distillation (8 kPa). Additionally, distance between primary and secondary nozzle is modified here in order to study its influence on the pump performance.

In [19], a newly designed jet pump was compared with two existing classical designs in terms of three performance parameters: mass flow ratio (drag coefficient), pressure ratio (quotient between the subtraction of discharge and suction pressures and the subtraction of drive nozzle and discharge pressures) and efficiency (multiplication of the former two parameters). The RNG $k-\varepsilon$ model with scalable wall functions for near wall treatment of ANSYS CFX™ was used for fluid-dynamics simulations, obtaining a better global performance for the new design. Three different cases were considered in the mentioned work [19] changing the inlet mass flow rate and keeping constant the remaining boundary conditions; then, for one of these cases, an erosion analysis was carried out combining a particle-tracking model for trajectory of sand particles and the Finnie's model for erosion prediction. In the present work, the parametric analysis developed comprises 18 working cases and considers a pressure type condition at the primary nozzle. A comparison between four different turbulence models commonly used in fluid-dynamics simulations of jet pumps, namely, standard $k-\varepsilon$ realizable $k-\varepsilon$, $k-\omega$ STT and RMS, was carried out in [20], finding that, according to experimental tests, the $k-\omega$ STT was the most suitable model for the working conditions considered there. One of the most important contributions of that work was the development of a method to estimate the location and shape of the shock-mixing layer; this allowed approximating the point along the pump length where the secondary and primary fluid fully mix each other. On the other hand, some authors [21] carried out a flow analysis of a fuel ejector pump using CFD, in order to systematically determine the appropriate values of constants of the standard $k-\varepsilon$ turbulence model. Considering that the standard $k-\varepsilon$ turbulence model is widely employed in fluid dynamic simulations of jet pumps, this is used in the present work.

In 2013, William Orozco [22,24], co-author of the present work, developed a unidirectional analytical model to obtain the optimum geometry and dimensions of a jet pump used in vacuum distillation of ethanol; this distillation consists of lowering the pressure and the temperature at which ethanol azeotropically distills, that is, using pressures below 101.3 kPa and temperatures below 78.6 °C, ethanol azeotrope can break and distillation can occur to obtain mix- purities higher than 95/5% ethanol / water [23]. Fig.1b shows the industrial scheme of the use of a vacuum pump (jet pump).

The model developed in [22,24], allows finding, among other parameters, the ideal diameter of the nozzle throat in order to generate a vacuum pressure of 8 kPa in the secondary fluid, for certain conditions of pressure and mass flow rate of the primary fluid, and keeping constant the drag coefficient in $w=0.5$. The general behavior of the fluid flow along the jet pump, in terms of the pressure and Mach number, as obtained from the previously developed 1D model, can be observed in (Fig.1a). The present work is focused on performing CFD simulations of a jet pump used in the vacuum distillation of ethanol, using the standard $k-\varepsilon$ turbulence model and the classical mass and energy conservation equations, for several purposes. Firstly, to compare the 1D analytical model previously developed in [22,24] with three-dimensional CFD simulations to assess whether the simplifications and assumptions of the 1D analytical model are pertinent in light of the more realistic, CFD results; it is evaluated the reliability of the more simplistic, analytical model to determine the optimum geometry and the field variables behavior of the jet pump. The second purpose of CFD simulations is to perform a parametric analysis about the influence of two critical parameters, such as the primary or motive fluid pressure (inlet pressure) and the location of the primary nozzle regarding the secondary one, in the pump performance. The pump performance is studied in terms of the drag coefficient and the behavior of the match number and total pressure over the fluid domain.



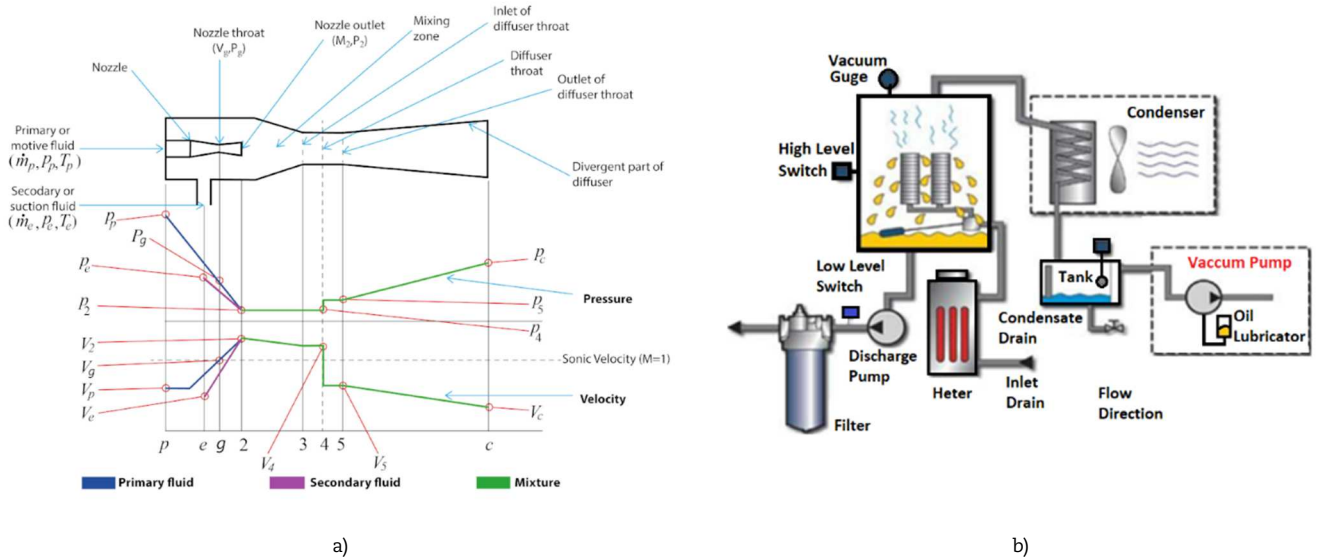


Fig. 1. a) Scheme of basic parts and field variables behavior of jet pump [22,24] b) Industrial scheme of the use of a vacuum pump (jet pump) [23]

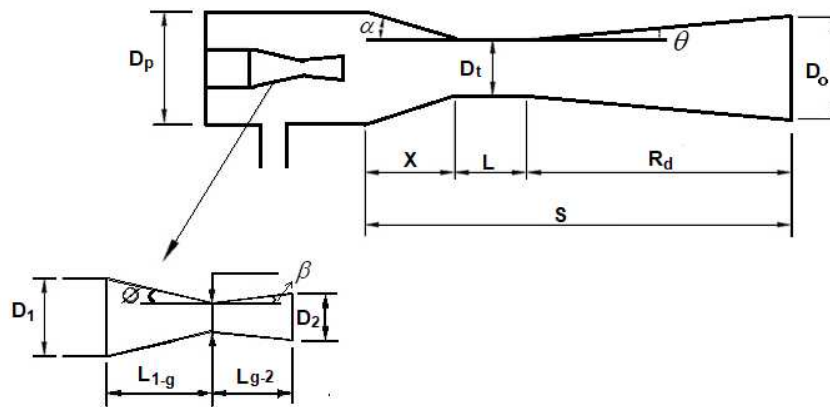


Fig. 2. Main dimensions for the geometric characterization of the jet pump [22].

2. Analysis Methodology

2.1. Unidirectional analytical modeling

In 2013, Orozco et al. [22,24] developed a 1D analytical model of a jet pump based on classical models for compressible gases, taking into account the characteristics of the primary and secondary fluids, as well as the variables involved in the vacuum distillation of ethanol. Using Matlab® software and following a methodology shown later, 1D simulations were performed using the developed model, finding the jet pump geometry that leads to optimum operating conditions. As a major contribution, results were compared with experimental tests previously reported in literature, finding errors lower than 10 %. Accordingly, the formerly obtained analytical model is employed here to define the geometric characteristics and determine the fluid flow behavior in a jet pump for vacuum distillation applications. The main assumptions of this model, as well as the literature that supports them, are summarized below:

- The pressure of both fluids (primary and secondary) at the mixing zone is the same; the best operating condition of the jet pumps is reached for that situation [25].
- Flow can be considered stationary and one-dimensional, since the primary and secondary fluid come from large containers [26].
- Fluid is adiabatic, since the pump can be considered thermally insulated [27].
- Wall shear stresses can be neglected in short Venturi tubes [28].
- Fluid in the pump behaves as ideal gas, since the air temperature is maintained in the range between 277.85 K and 558.65 K [28].
- Fluid is isentropic, because it traverses short sections in the convergent-divergent ducts, is adiabatic and frictionless [29].
- Both fluids are reversible from their respective origin to the zone where mixing takes place, since friction effects are neglected due to the short sections of the convergent-divergent ducts [28].
- Mixing is complete and the speed is supersonic at the inlet of diffuser throat; the best operating condition of the jet pumps is reached for that situation [29].
- Speed of compressed mixture at the diffuser outlet is negligible compared to the other speeds [29].
- The pressure of both fluids at the mixing zone is smaller than the lower flammability limit of ethanol to avoid an explosive mixture [30].



The geometric optimization of the jet pump is carried out in terms of the variables shown in (Fig. 2), whose meaning is mentioned in the nomenclature table at the end of the manuscript. This geometric optimization focuses on obtaining some pump dimensions to achieve a drag coefficient of $w=0.5$. The analytical procedure that allows calculating the optimum dimensions of some parts of the jet pump is shown in (Fig. 3a). Details of this procedure can be found in [22,24].

Summary of equations corresponding to procedure shown in (Fig. 3a) is presented as follows:

$$A_g = \frac{\rho_p A_p V_p}{V_g \rho_g} \quad (1)$$

$$V_p = \frac{\dot{m}}{A_p \rho_p} \quad (2)$$

$$c = (kRT_g)^{1/2} \quad (3)$$

$$\frac{T_g}{T_p} = \left[\frac{2}{k+1} \right] \quad (4)$$

$$\frac{\rho_g}{\rho_p} = \left[\frac{2}{k+1} \right]^{\frac{1}{k-1}} \quad (5)$$

$$\dot{m}_{\max} = A_g P_0 \left[\frac{k}{RT_0} \left(\frac{2}{k+1} \right)^{\frac{k+1}{k-1}} \right]^{1/2} \quad (6)$$

$$M_{p2} = \left[\frac{2P_p}{RT_g \rho_p^{k-1}} \left(1 - \left(\frac{P_2}{P_p} \right)^{\frac{k-1}{k}} \right) \right]^{1/2} \quad (7)$$

$$\frac{A_2}{A_g} = \left[\frac{1}{M_{p2}^2} \left(\frac{2 + (k-1)M_{p2}^2}{k+1} \right)^{\frac{k+1}{k-1}} \right]^{1/2} \quad (8)$$

$$L_{1-g} > \frac{(D_1 - D_g)}{2} \quad (9)$$

$$L_{g-2} > \frac{(D_1 - D_g)}{\tan \beta} \quad (10)$$

$$A_4 = 10A_g \quad (11)$$

$$A_4 = \frac{\pi D_g^2}{4} \quad (12)$$

$$A_g = \frac{\pi D_g^2}{4} \quad (13)$$

$$L = 1,5D_g \quad (14)$$

$$R_d = \varsigma D_t \quad (15)$$

$$D_0 = 2R_d \tan \theta + D_t \quad (16)$$

$$X = \eta D_g \quad (17)$$

$$D_p = 2X \tan \alpha + D_t \quad (18)$$

On the other hand, the analytical procedure to obtain the fluid flow behavior of the jet pump, once its geometry is defined, is presented in (Fig. 3b). This procedure is based on the semi-empirical model of [29]. Details of this procedure can be found in [22,24]. Summary of equations corresponding to procedure shown in (Fig. 3b) is presented as follows:

$$M_{e2} = \left[\frac{2}{ks-1} \left(\frac{P_e}{P_2} \right)^{\frac{ks-2}{ks}} - 1 \right]^{1/2} \quad (19)$$



$$M_4^* = \frac{M_{p2}^* + wM_{e2}^* \left(\frac{T_e}{T_p} \right)^{1/2}}{\left[(1+w) \left(1 + w \left(\frac{T_e}{T_p} \right) \right) \right]^{1/2}} \tag{20}$$

$$M_4^* = \left[\frac{M_4^2 (k_m + 1)}{M_4^2 (k_m - 1) + 2} \right]^{1/2} \tag{21}$$

$$M_5 = \frac{M_4^2 + \frac{2}{k_m - 1}}{2k_m M_4^2 - 1} \tag{22}$$

$$\frac{P_5}{P_4} = \frac{1 + k_m M_4^2}{1 + k_m M_5^2} \tag{23}$$

$$\frac{P_c}{P_5} = \left[\left(\frac{k_m - 1}{2} M_5^2 \right) + 1 \right]^{\frac{k_m}{k_m - 1}} \tag{24}$$

2.2. Computational fluid dynamics analysis

2.2.1. Geometric modeling and material definition

The modeling of the fluid domain was carried out in the CAD software SolidWorks, considering the geometry and dimensions of a jet pump for ethanol distillation previously obtained in [22]. The basic geometry and dimensions of the jet pump can be observed in (Fig. 4a and 4b); distance between primary and secondary nozzle, X_p , which is considered variable in the present study, is represented in (Fig. 4b). In addition, it can be seen that only half of the fluid domain was modeled considering that the pump is symmetric with respect to a longitudinal plane. Regarding some geometric details and their effect on the results, it is important to highlight that considering a large number of details may result in a higher computational cost due to the appearance of numerical singularities, without significantly improving the accuracy of numerical results. Therefore, geometry shown in (Fig. 4b) obviates some constructive details of the jet pump without affecting the numerical analysis.

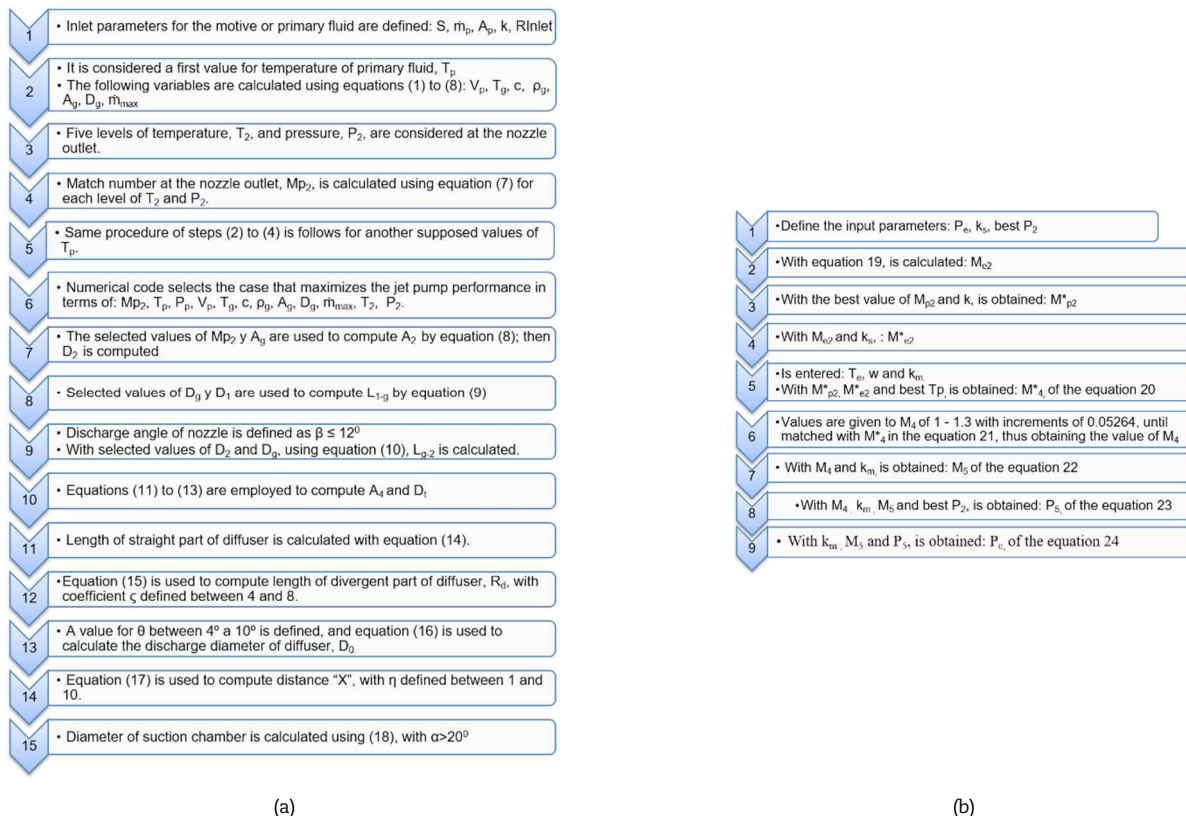


Fig. 3. a) Analytical procedure to obtain optimum dimensions of jet pump, b) Procedure to obtain non-dimensional fluid flow variables of the jet pump [18].



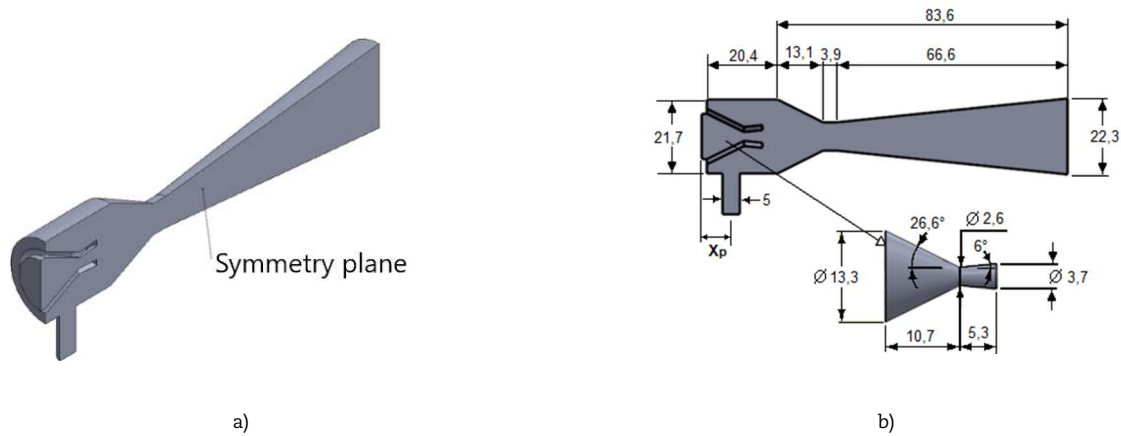


Fig. 4. a) Symmetry plane of jet pump, b) Basic geometry and dimensions for CFD simulations.

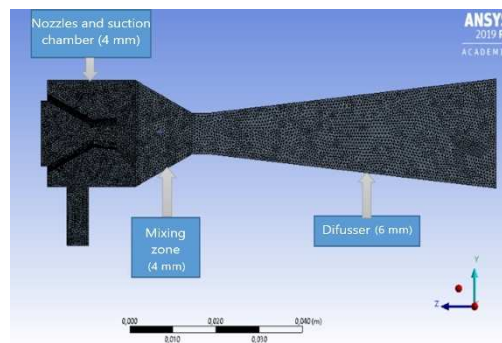


Fig. 5. Mesh size of fluid domain.

Computational fluid dynamics simulations were carried out in ANSYS Fluent™. It was considered an air domain governed by the ideal gas law, whose properties are: specific heat of $C_p=1006.43$ J/kgK, thermal conductivity of $K=0.0242$ W/mk, viscosity of $\mu=1.79E-05$ kg/ms, molecular weight of 28.96 g/mol. In the present work, as in the ones published in [22,24], species transport phenomenon is not simulated (ethanol + air + water mixture), but it is considered an air domain where the suction pressure of the secondary fluid must be maintained at 8 kPa to permit ethanol distillation.

2.2.2. Definition and analysis of mesh quality

The size and quality of the mesh elements must guarantee the convergence and stability of the numerical solution. In this particular case, the type of element used for the fluid domain is linear tetrahedral, with three different mesh sizes: 4 mm in the nozzle zone and the suction chamber, 4 mm in the mixing section and 6 mm in the diffuser, as can be seen in (Fig. 5). The total number of finite volumes and nodes are 409181 and 80313, respectively. The characteristics of this mesh were obtained after performing a convergence analysis, which can be seen in (Fig. 6a), where the L^2 relative error norm for the Mach numbers and the computation time, in terms of the number of nodes, are reported. In this case, L^2 relative error norm is computed as follows:

$$L^2 = \sqrt{\frac{\sum_{j=1}^m (Ma_j^{(2)} - Ma_j^{(1)})^2}{\sum_{j=1}^m (Ma_j^{(1)})^2}} \quad (25)$$

where $Ma_j^{(2)}$ and $Ma_j^{(1)}$ are the Mach number at point "j" of the fluid domain corresponding to two subsequent mesh configurations represented by 2 (finer mesh) and 1 (rougher mesh), respectively, whereas m is the number of points used to compute L^2 , which, in the present case, are taken as the points of the finer mesh. As can be seen in (Fig. 6a), an increase from the selected mesh (80313 nodes) to the immediately superior mesh (145673 nodes) means a variation in the L^2 relative error norm of 37.92%, at the expense of an increment in the computation time of 172.34%, indicating that this mesh refinement is not practical.

The mesh quality is evaluated in this work considering the mesh skewness. This mesh quality parameter indicates how similar the actual element is to an ideal element; in this case, an ideal element is an equilateral tetrahedron. Skewness of zero indicates that the element is ideal, while a skewness of one means that all nodes of the element are coplanar (this is known as degenerate element). Table 1 shows the elements assessment according to their skewness. For tetrahedral elements, skewness is obtained as:

$$Skewness = \frac{(V_{opt} - V_{real})}{V_{opt}} \quad (26)$$

where V_{real} is the volume of real element, while V_{opt} is the optimal volume, defined as the volume of an ideal element with the same circumradius to the real element. As can be seen in (Fig. 6b), most of the elements are in the range of excellent to moderate, which denotes an acceptable mesh quality that can lead to acceptable interpolation errors.



Table 1. Assessment of element quality according to the skewness.

Skewness Value	Element Classification
0	Ideal
>0-0.25	Excellent
0.25-0.5	Good
0.5-0.75	Moderate
0.75-0.9	Moderate to bad
0.9-<1	Bad
1	Degenerate

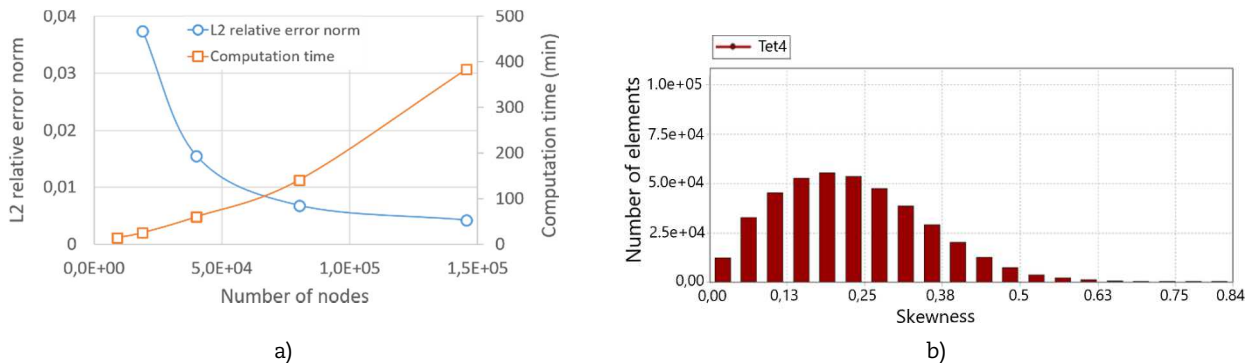


Fig. 6. a) L² relative error norm and computation time for CFD mesh, **b)** Skewness distribution of mesh element.

2.2.3. Governing equations, reference values and convergence monitors

Three types of governing equations must be taken into account in the computational simulations of the jet pump: mass conservation, momentum conservation (k-ε turbulence model) and energy conservation. The standard mass conservation equation used in ANSYS Fluent™ is as follows:

$$\frac{\delta \rho}{\delta t} + \nabla \cdot (\rho \vec{v}) = S_m \tag{27}$$

where ρ, \vec{v} and S_m represent density, velocity vector and a source term to quantify mass transfer between phases (which is null in this case), respectively. On the other hand, the energy equation solved by ANSYS Fluent™ has the following generic form:

$$\frac{\delta(\rho E)}{\delta t} + \nabla \cdot (\vec{v}(\rho E + P)) = \nabla \cdot [K_{eff} \nabla T - \sum_j h_j \vec{J}_j + (\vec{\tau}_{eff} \cdot \vec{v})] + S_h \tag{28}$$

where E is the total energy, K_{eff} is the effective thermal conductivity (incorporates the turbulent thermal conductivity), h_j and \vec{J}_j represent the enthalpy and diffusive flux of species (null in this case), $\vec{\tau}_{eff} \cdot \vec{v}$ is the dissipation viscous term and S_h is the source term. The above energy equation already contains the coupling between fluid velocity and static temperature, and it is not necessary to activate this manually. As mentioned above, the k-ε turbulence model has been previously used for fluid-dynamic simulations of jet pumps [4][5][7][14,15]. The governing equations of this model are shown below:

$$\frac{\delta}{\delta t} (\rho k) + \frac{\delta}{\delta x_i} (\rho k u_i) = \frac{\delta}{\delta x_j} \left[\left(\mu + \frac{\mu_t}{\sigma_k} \right) \frac{\delta k}{\delta x_j} \right] + G_k + G_b - \rho \varepsilon - Y_M + S_k \tag{29}$$

$$\frac{\delta}{\delta t} (\rho \varepsilon) + \frac{\delta}{\delta x_i} (\rho \varepsilon u_i) = \frac{\delta}{\delta x_j} \left[\left(\mu + \frac{\mu_t}{\sigma_\varepsilon} \right) \frac{\delta \varepsilon}{\delta x_j} \right] + C_{1\varepsilon} \frac{\varepsilon}{k} (G_k + C_{3\varepsilon} G_b) - C_{2\varepsilon} \rho \frac{\varepsilon^2}{k} + S_\varepsilon \tag{30}$$

where k is the turbulent kinetic energy and ε is its corresponding dissipation rate, whereas G_k and G_b are generation terms of turbulence kinetic energy, the first one associated to the average velocity gradients and the second one, to buoyancy. The velocity field is represented by u_i, the density by ρ and the turbulent viscosity by μ_t. The latter is calculated using the following equation:

$$\mu_t = \rho C_\mu \frac{k^2}{\varepsilon} \tag{31}$$

On the other hand, Y_M represents the contribution of fluctuating dilatation to the overall dissipation rate, while C_{1ε}, C_{2ε} and C_{3ε} are characteristic constants of the model. Due to the presence of supersonic flows in some zones of the pump, the air compressibility can significantly affect the turbulence field variables. For that reason, it should be assured that term Y_M is present during the whole simulation by activating the compressibility correction offered by ANSYS Fluent™ [31]. On the other hand, Prandtl numbers for k and ε are α_k and α_ε respectively, while S_k and S_ε are source terms. More details about the meaning of these parameters can be found in [32,33]. Default values of some parameters are considered in these simulations, that is: C_{1ε} = 1.44, C_{2ε} = 1.92, C_μ = 0.09, α_k = 1.0 and α_ε = 1.3. To relate the solution variables in the cells adjacent to walls with the corresponding variables of the walls, ANSYS Fluent™ software has several semi-empirical formulae for the average velocity, temperature and turbulent quantities, called Wall Functions. For the present simulations, the standard wall functions proposed by Launder and Spalding are selected [34,35]. The reference values used in the computation of the derived physical quantities and the dimensionless coefficients in the postprocessing stage are: density of 7 kg/m³; area of 1 m²; enthalpy of 0 J/kg; viscosity of 1.79E-05 kg/ms; length of 1 m; pressure of 0 Pa; temperature of 288.16 K; velocity 1 of m/s; ratio of specific heats of 1.4. On the other hand, the convergence monitors and their respective allowable residuals are: Continuity (1E-06); Velocity-X (1E-06); Velocity-Y (1E-06); Velocity-Z (1E-06); Energy (1E-06); K



parameter (1E-06); Epsilon parameter (1E-06).

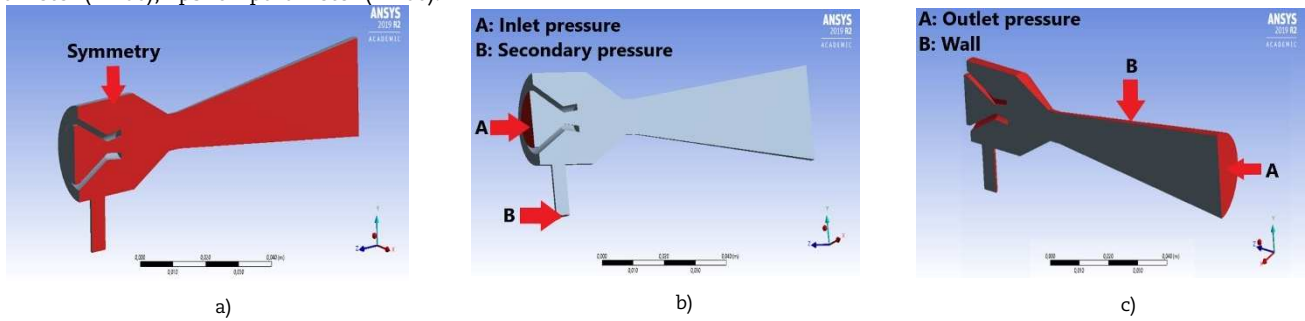


Fig. 7. Boundary conditions of CFD simulation. a) Symmetry, b) Inlet and secondary pressures, c) Outlet pressure and wall-type condition.

2.2.4. Prescription of boundary conditions

Boundary conditions are prescribed at the domain faces as shown in (Fig. 7a-c). Symmetry condition is considered in the longitudinal plane of the pump, where normal flow and tangential tractions are zero (Fig. 7a). At inlet of primary fluid, absolute pressure condition is assigned (Fig. 7b), which was modified from 50 kPa to 300 kPa, at 50 kPa intervals, to perform a parametric study. In that inlet, air temperature of 298 K is considered. Additionally, the option “Prevent reverse flow” is activated to avoid backflows during iterations that can disrupt the numerical solution. For the turbulence intensity of the k-ε model, a value of 5% is considered. On the other hand, absolute pressure of 8 kPa is assigned at the inlet of secondary fluid (Fig. 7b). Air temperature of secondary fluid is considered as 295K, “Prevent reverse flow” control is assigned as well, and turbulence intensity value of 5% is considered. Over the face corresponding to diffuser outlet (Fig. 7c), initial pressure condition of 4.5 kPa, temperature of 295K and turbulence intensity of 5% are assigned, but these conditions are modified as the simulation is executed, according to the governing equations. Finally, a wall-type condition (sliding and zero penetration) is prescribed over the external faces of the domain (Fig. 7c).

2.2.5 Initialization and solution methods

To initialize the numerical solution, a hybrid scheme with 20 iterations and the default turbulence parameters of software for the k-ε turbulence model (turbulence intensity of 5% and viscosity ratio of 10) is used. A coupled Pressure-Velocity solution scheme is selected, with a second order, upwind spatial discretization method for scalar variables (pressure, density, momentum, turbulent kinetic energy, turbulent dissipation rate and total energy) and gradient calculation by least squares based on cells. The relaxation factors used in the numerical simulation are: 0.5 for pressure; 0.5 for moment; 1 for density; 1 for body forces; 0.75 for turbulent kinetic energy; 1 for turbulent dissipation rate; 0.75 for Energy.

2.2.6. Set of computational simulations

The position of the primary nozzle with respect to secondary one, represented in (Fig. 4b) by X_p , is modified in order to study the influence of such position on the performance and fluid flow behavior of the jet pump. Three positions are considered, that is, $X_p = [8.5 \text{ mm}, 10.5 \text{ mm}, 12.5 \text{ mm}]$, and for each one, 6 simulations are performed corresponding to the following inlet pressures of the primary fluid: $P_p = [50, 100, 150, 200, 250, 300] \text{ kPa}$. An additional CFD simulation, for comparison purposes with analytical results, is performed with an inlet pressure of 70 kPa, where a drag coefficient very close to $w = 0.5$ is achieved. In all simulations, inlet pressure of the secondary fluid is maintained at $P_s = 8 \text{ kPa}$ and pressure at diffuser outlet at $P_c = 4.5 \text{ kPa}$.

Several works of fluid-dynamic simulation of jet pumps focused on studying their performance are presented in Table 2, where input and output parameters, boundary condition types, numerical methods, turbulence models and solution settings are identified; the principal characteristics of the CDF simulations performed here are reported as well in order to show the principal differences and similitudes with previous works. As can be observed, there are some common aspects between present work and other researches: the substantial use of k-ε turbulence models and ANSYS Fluent to carry out the numerical simulations, the use of pressure type boundary conditions for the motive, suction and discharge fluid, the implementation of coupled pressure-velocity solution scheme and pressure-based solver type in most of works, among others. Nevertheless, some differences between present work and other researches allow identifying the main contributions. Firstly, in the present work, the influence of the combination of two input parameters on the jet pump performance is taken into account, namely, the motive fluid pressure and the position of the primary nozzle; as can be observed in some works of Table 2, these parameters have been previously considered by apart, but not at the same time. Additionally, output parameters considered here to quantify the jet pump performance are drag coefficient (mass flow ratio), inlet to nozzle throat pressure ratio and nozzle throat velocity. As can be seen in Table 2, the first parameter has been widely used in other works, but this is not enough to evaluate the Venturi effect arising in the jet pump and two additional parameters are considered here; as shown later, the increase of drag coefficient does not necessarily imply the increase of the other two parameters since several phenomena involved in the jet pump performance are not deemed by this first non-dimensional parameter (mass flow ratio). The detailed analysis of Mach number and total pressure contours to determine whether jet pump is operating or not under normal conditions for any combination of primary nozzle position and inlet pressure signifies another contribution of the present work.

Table 2. Summary of works of fluid-dynamic simulation of jet pumps.

Research work	Input parameters	Output parameters	Boundary condition types	Numerical method	Turbulence models	Solution settings
Present work	* Primary or motive fluid pressure * Position of primary nozzle	* Mass flow ratio or drag coefficient. * Ratio between inlet and nozzle throat pressure. * Nozzle throat velocity * Mach number and total pressure contours	* Primary or motive fluid: Pressure. * Secondary or suction fluid: Pressure * Discharge fluid: Pressure	Finite volume method (ANSYS Fluent)	k-ε standard	* Solution scheme: Coupled pressure-velocity * Solver type: Pressure-based * Spatial discretization: Second order upwind * Near Wall treatment: Standard wall functions * Gradient calculation: Least squares based on cells



Table 2. Summary of works of fluid-dynamic simulation of jet pumps. (Continued)

Research work	Input parameters	Output parameters	Boundary condition types	Numerical method	Turbulence models	Solution settings
Yapici and Aldas [16]	* Jet pump area ratio. * Nozzle position. * Length of the mixing chamber.	Energy efficiency	* Primary or motive fluid: Pressure. * Secondary or suction fluid: Pressure * Discharge fluid: Pressure	Finite volume method (ANSYS Fluent)	* k- ϵ standard * k- ϵ realizable * RSM * k- ω SST	* Solution scheme: Coupled pressure-velocity * Solver type: Pressure-based * Spatial discretization: Quick scheme * Near Wall treatment: Not reported * Gradient calculation: Not reported
Aldas and Rapici [17]	* Pump scaling * Absolute and relative roughness	Energy efficiency	* Primary or motive fluid: Pressure. * Secondary or suction fluid: Pressure * Discharge fluid: Pressure	Finite volume method (ANSYS Fluent)	k- ω SST	* Solution scheme: Coupled pressure-velocity * Solver type: Pressure-based * Spatial discretization: Second order, upwind * Near Wall treatment: Standard wall function * Gradient calculation: Least square cell-based method
Shah, Chughtai and Inayat [18]	* Primary or motive fluid pressure * Secondary or suction fluid pressure	* Mass flow ratio or drag coefficient * Suction lift	* Primary or motive fluid: Pressure. * Secondary or suction fluid: Pressure * Discharge fluid: Pressure	Finite volume method (ANSYS Fluent)	k- ϵ realizable	* Solution scheme: Coupled pressure-velocity * Solver type: Simple couple implicit * Spatial discretization: First order and second order, upwind, and Power law * Near wall treatment: Not reported * Gradient calculation: Least square cell-based method
Song et al. [19]	Inlet mass flow rate	* Mass flow ratio or drag coefficient * Pressure ratio * Efficiency	* Primary or motive fluid: Mass flow rate * Secondary or suction fluid: Pressure * Discharge fluid: Pressure	Finite volume method (ANSYS CFX)	RNG k- ϵ model	* Solution scheme: Coupled pressure-velocity * Solver type: Not reported * Spatial discretization: Not reported * Near Wall treatment: Scalable wall function * Gradient calculation: Not reported
Dong, Wang and Tu [20]	Back pressure	Location and shape of shock mixing layer	* Primary or motive fluid: Pressure. * Secondary or suction fluid: Pressure * Discharge fluid: Pressure	Finite Volume method (ANSYS Fluent)	* k- ϵ standard * k- ϵ realizable * RSM * k- ω SST	* Solution scheme: Coupled pressure-velocity * Solver type: Simple coupled implicit * Spatial discretization: Second order upwind for convection terms and central difference scheme for diffusion * Near Wall treatment: Enhanced wall functions * Gradient calculation: Not reported
Zheng, Li and Qin [4]	* Inlet velocity of primary fluid * Secondary or suction fluid pressure * Mixture outlet pressure	* Axial velocity * Volume ratio of primary and secondary fluid * Axial temperature * Entrainment ratio	* Primary or motive fluid: Velocity * Secondary or suction fluid: Pressure * Discharge fluid: Pressure	Finite volume method (ANSYS Fluent)	k- ϵ standard	* Solution scheme: Coupled pressure-velocity * Solver type: Pressure-based * Spatial discretization: Body force weighted for pressure, second order upwind for momentum, energy and turbulent kinetic * Near Wall treatment: Standard wall functions * Gradient calculation: Not reported
Deng et al. [5]	Geometry of mixing chamber	Air entrainment	* Primary or motive fluid: Velocity * Secondary or suction fluid: Velocity * Discharge fluid: Pressure	Finite Volume Method (ANSYS Fluent)	* k- ϵ standard * k- ϵ realizable * k- ϵ RNG	* Solution scheme: Coupled pressure-velocity * Solver type: Simple coupled implicit * Spatial discretization: Second order upwind * Near Wall treatment: Standard wall functions * Gradient calculation: Not reported
Varga et al. [6]	Inlet cross section of primary nozzle	* Primary flow rate * Secondary flow rate	* Primary or motive fluid: Pressure * Secondary or suction fluid: Pressure * Discharge fluid: Pressure	Finite Volume (ANSYS Fluent)	k- ϵ realizable	* Solution scheme: Coupled pressure-velocity * Solver type: Pressure-based * Spatial discretization: Not reported * Near Wall treatment: Not reported * Gradient calculation: Not reported



Table 2. Summary of works of fluid-dynamic simulation of jet pumps. (Continued)

Research work	Input parameters	Output parameters	Boundary condition types	Numerical method	Turbulence models	Solution settings
Thongtip and Aphornratana [12]	* Area ratio of primary nozzle * Throat diameter	* Primary flow rate * Secondary flow rate * Entrainment ratio * Mach number contours	* Primary or motive fluid: Pressure * Secondary or suction fluid: Pressure * Discharge fluid: Pressure	Finite volume method (ANSYS Fluent)	k- ϵ realizable	* Solution scheme: Coupled pressure-velocity * Solver type: Density-based implicit * Spatial discretization: Not reported * Near Wall treatment: Standard wall fraction * Gradient calculation: Not reported
Masud and Inram [21]	Constant parameters of k- ϵ standard model	* Primary flow rate * Discharge flow rate	* Primary or motive fluid: Pressure * Secondary or suction fluid: Pressure * Discharge fluid: Pressure	Finite volume method (ANSYS Fluent)	k- ϵ standard	* Solution scheme: Coupled pressure-velocity * Solver type: Pressure-based implicit * Spatial discretization: Not reported * Near Wall treatment: Standard wall function * Gradient calculation: Not reported

Table 3. Comparison between analytical and CFD results of some non-dimensional variables.

Dynamic variable	Unidirectional analytical model	CFD simulation	Relative difference, d (%)
M_{e2}	1.867E+00	1.515E+00	23.241
M_4	1.263 E+00	1.763E+00	28.329
M_5	6.420 E-01	9.930E-01	35.347
P_5/P_4	1.980 E+00	1.451E+00	36.427

3. Results

3.1. Comparison between unidirectional analytical model and the CFD numerical simulations.

As previously discussed in section 2.1, the unidirectional analytical model provides two types of results: some optimal dimensions of the jet pump to obtain an ideal drag coefficient of $w=0.5$ under certain operating conditions (Fig. 3a), and some field variables that describe the fluid flow behavior of jet pump (Fig. 3b). In the CFD simulations, for the position of $X_p = 8.5$ mm and inlet pressure of primary fluid of 70 kPa, a drag coefficient of $w = 0.5$ is obtained. If the same pump operating conditions are considered in the analytical model and it is iterated over the mass flow rate of the primary fluid, $\dot{m}_{in,anal}$, to obtain similar pump dimensions to the ones considered in the CFD simulations, a value of $\dot{m}_{in,anal} = 7.790 \times 10^{-4}$ kg/s is reached using procedure of (Fig. 3a). On the other hand, the value of this variable in the CFD simulation is $\dot{m}_{in,CFD} = 8.586 \times 10^{-4}$ kg/s. Defining the relative difference as $d = |\dot{m}_{in,anal} - \dot{m}_{in,CFD}| / \dot{m}_{in,CFD} \times 100\%$, a value of $d = 9.15\%$ is obtained, showing that analytical model, despite its simplicity, is able to obtain similar results to the more complex 3D, CFD simulations for this global variable. Then, using analytical procedure of (Fig. 3b), the following non-dimensional local variables can be computed: Mach number of secondary fluid at nozzle outlet (M_{e2}), maximum Mach number of diffuser throat (M_4), Mach number at outlet of diffuser throat (M_5) and ratio between pressure at outlet and minimum pressure of diffuser throat (P_5/P_4). In the 1D, analytical model, these local variables are constant in the transverse plane, but in the 3D, CFD simulations, changes are obtained in such plane; for comparison purposes, averages are reported for the CFD variables. Bearing this in mind, in Table 3, the analytical and CFD values of these four non-dimensional variables are compared in terms of the previously defined relative difference, d . As observed, important differences are obtained between the 1D, analytical model and the 3D, CFD simulation, but some common behaviors are predicted by both approaches. For instance, the maximum Mach number, M_4 , is not present at inlet or outlet of diffuser throat, but at an intermediate location where a supersonic fluid flow is obtained, i.e., $M_4 > 1$. Additionally, according to value of M_5 in both approaches, subsonic fluid flow is reached at outlet of diffuser throat. On the other hand, both approaches predict that minimum pressure at diffuser throat, P_4 , coincides with maximum Mach number, M_4 (this is not obvious in this case since fluid flow is compressible); in addition, ratio P_5/P_4 has the same magnitude order in both approaches (analytical and numerical), in spite of the difference of $d=36.43\%$. As shown later in the CFD contour plots of Mach number and total pressure, significant transverse variations of the local variables can be obtained in some longitudinal locations of the pump domain, being this one the main causes of dissimilarities between the analytical and numerical results.

3.2. Influence of position and pressure of primary nozzle on the performance of the jet pump

One of the fundamental parameters to quantify the performance of the jet pump is the drag coefficient (w), defined as the ratio between the mass flow rate of secondary fluid (suction flow rate) and the mass flow rate of primary fluid (motive flow rate). These mass flow rates were obtained directly from the computational simulation in ANSYS Fluent™ for each one of the pressures and positions of the primary nozzle, achieving the results shown in the (Fig. 8). As can be observed, X_p does not have a significant effect on w , which decreases with P_p . In (Fig. 8), a power fitting curve for all data is shown, with its respective coefficient of determination, R^2 . According to the value of R^2 , the behavior of w with P_p can be considered decreasing potential. As expected from the power curve behavior, the decrease of w with P_p is more important as P_p is smaller. For example, when P_p increases from 50kPa to 100kPa, w experiences an average decrease of 51%, whereas when the same absolute increment is considered for P_p , but this time from 250 kPa to 300 kPa, the average decrease of w is 24.61%. It is worth noting that for the present geometric configuration of the jet pump, CFD simulations generate very low values of w for inlet pressures greater than 250 kPa.



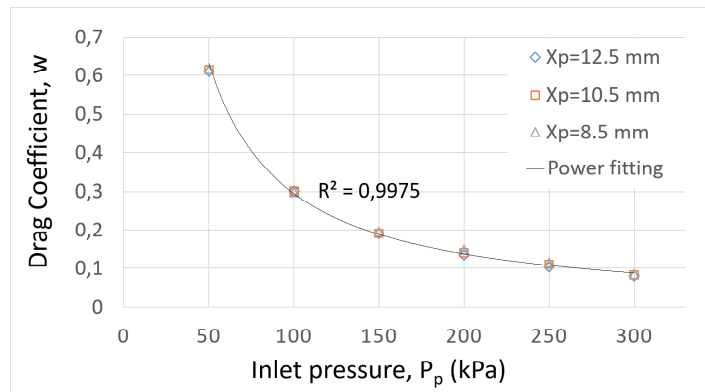


Fig. 8. Plots of drag coefficient (w) vs. Inlet pressure (P_p).

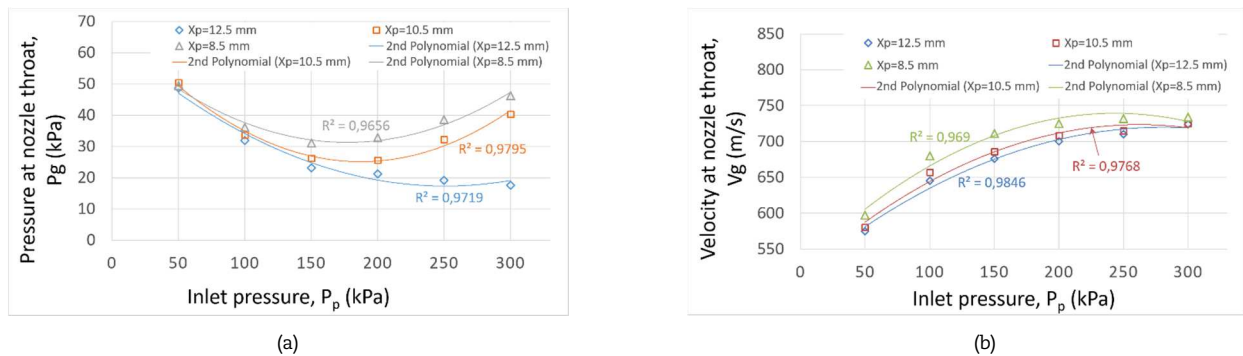


Fig. 9. a) Pressure at nozzle throat (P_g) vs. Inlet pressure (P_p), b) Velocity at nozzle throat (V_g) vs. Inlet pressure (P_p).

Another important parameter in the performance of the jet pump is the pressure at the nozzle throat, P_g . Results of P_g as a function of P_p and X_p , are represented in the (Fig. 9a). The fitting curves that adjust well the behavior of P_g vs. P_p are second order polynomial curves. In general terms, the variation of P_g with P_p depends on X_p , being decreasing for $X_p = 12.5$ mm, and not monotonous for $X_p = 10.5$ mm and $X_p = 8.5$ mm. In general, the Venturi effect for very low inlet pressures (from 50 kPa to approximately 75 kPa) is very small, since ratio P_p/P_g is below 2, which indicates that although the drag coefficients, w , are the higher for these pressures, see (Fig. 8), secondary fluid suction is not caused mainly by the Venturi effect, but instead by the low inlet pressure of the primary fluid. Given this condition, although w is good, the mass flow rates are very small. For P_p between 75 kPa and 100 kPa, the ratio P_p/P_g ranges between 2 and 3 and drag coefficients remain above $w = 0.3$, which can be considered acceptable. For P_p between 100 kPa and 150 kPa, Venturi effect is more significant (P_p/P_g is between 3 and 6.5), but drag coefficients are lower. From 150 kPa onwards, a significant Venturi effect is present (P_p/P_g is between 6.5 and 16.5), but drag coefficients are very small for the jet pump to be considered efficient. In (Fig. 9a) it is also important to notice that the position of the primary nozzle, X_p , has a greater influence on the pressure obtained in the nozzle throat, P_g , as the inlet pressure, P_p , increases. In general, for a same value of P_p , the larger the distance between the primary and secondary nozzle, X_p , the lower the pressure in the nozzle throat, P_g , namely, the higher the Venturi effect (P_p/P_g).

Another important parameter to evaluate the performance of a jet pump is the fluid velocity at the nozzle throat, V_g . According to several authors [12, 13, 18, 21, 23], an acceptable performance of the jet pump occurs when V_g is supersonic. In (Fig. 9b), the variation of V_g with P_p is shown, and data fit well to second order polynomial curves. The larger the inlet pressure, P_p , the higher the nozzle throat velocity, V_g . Regarding the distance between primary and secondary nozzle, X_p , numerical results indicate that the closer the primary nozzle is to secondary one, the higher the nozzle throat velocity, V_g , although in this case, results for $X_p = 10.5$ mm and $X_p = 12.5$ mm are slightly different.

3.3. Influence of position and pressure of primary nozzle in Mach number and total pressure.

To evaluate the influence of the position and pressure of the primary nozzle on the Mach number, the contour plots in the symmetry plane shown in (Fig. 10) are analyzed; in that Figure, rows refer to the pressure levels considered and the columns, to position of primary nozzle, X_p . It can be observed that for pressures of 50 kPa and 100 kPa, for all positions of the primary nozzle, X_p , the maximum Mach number takes place at the diffuser outlet, which does not correspond to normal operating conditions of the jet pump. For these inlet pressures, the distribution of Mach number field does not change significantly with the position of the primary nozzle, with exception of some localized zones; however, magnitudes of Mach number are noticeably modified. In general, the closer the primary nozzle is to the secondary one, the greater the Mach number at the diffuser outlet. In addition, it is observed that the minimum Mach number is present at the inlet of primary nozzle and, contrarily to maximum Mach number, it does not have a monotonic behavior with X_p , since the smallest value is obtained for the intermediate position ($X_p = 10.5$ mm). It should be noticed that for these cases, flow in the throat is supersonic. Similarly, pressures of 150 kPa and 200 kPa are analyzed, where it can be perceived that maximum Mach number occurs between the outlet of the convergent-divergent nozzle and the inlet of the diffuser throat (jet pump operating in normal conditions). For these two inlet pressures (150 kPa and 200 kPa), an increase in the Mach number is generated in the nozzle throat with respect to previously analyzed pressures of 50 kPa and 100 kPa. As in cases of 50 kPa and 100 kPa, the minimum Mach number is present at the inlet of primary nozzle and its change with X_p is non-uniform. In a similar fashion as cases of 50 kPa and 100 kPa, the maximum Mach number increases as the primary nozzle is closer to secondary one. Additionally, for 150 kPa and 200 kPa, the throat flow is supersonic as well.

For all cases corresponding to inlet pressures of 250 kPa and 300 kPa, the maximum Mach number also occurs between the outlet of the convergent-divergent nozzle and the inlet of the diffuser throat, but in these two cases, Mach numbers obtained at diffuser outlet are significantly lower than maximum Mach numbers of the domain (contrarily to cases of 150 kPa and 200 kPa). It



is important to notice that the behavior of maximum Match number with the position of primary nozzle, X_p , is different for 250 kPa and 300 kPa. In the first case (250 KPa), in agreement with all the previous cases, this value is larger as the primary nozzle is closer to the secondary one, but, in the second case (300 kPa), an opposite behavior is obtained. The minimum Mach number is still present at the inlet of primary nozzle and its behavior with X_p is kept, namely, it is not monotonic. Nozzle throat velocity, V_g , remains supersonic. In (Fig. 10), it can be also observed that, for a given position of the primary nozzle, X_p , the increase in P_p generates an increase in the maximum Match number of the fluid domain.

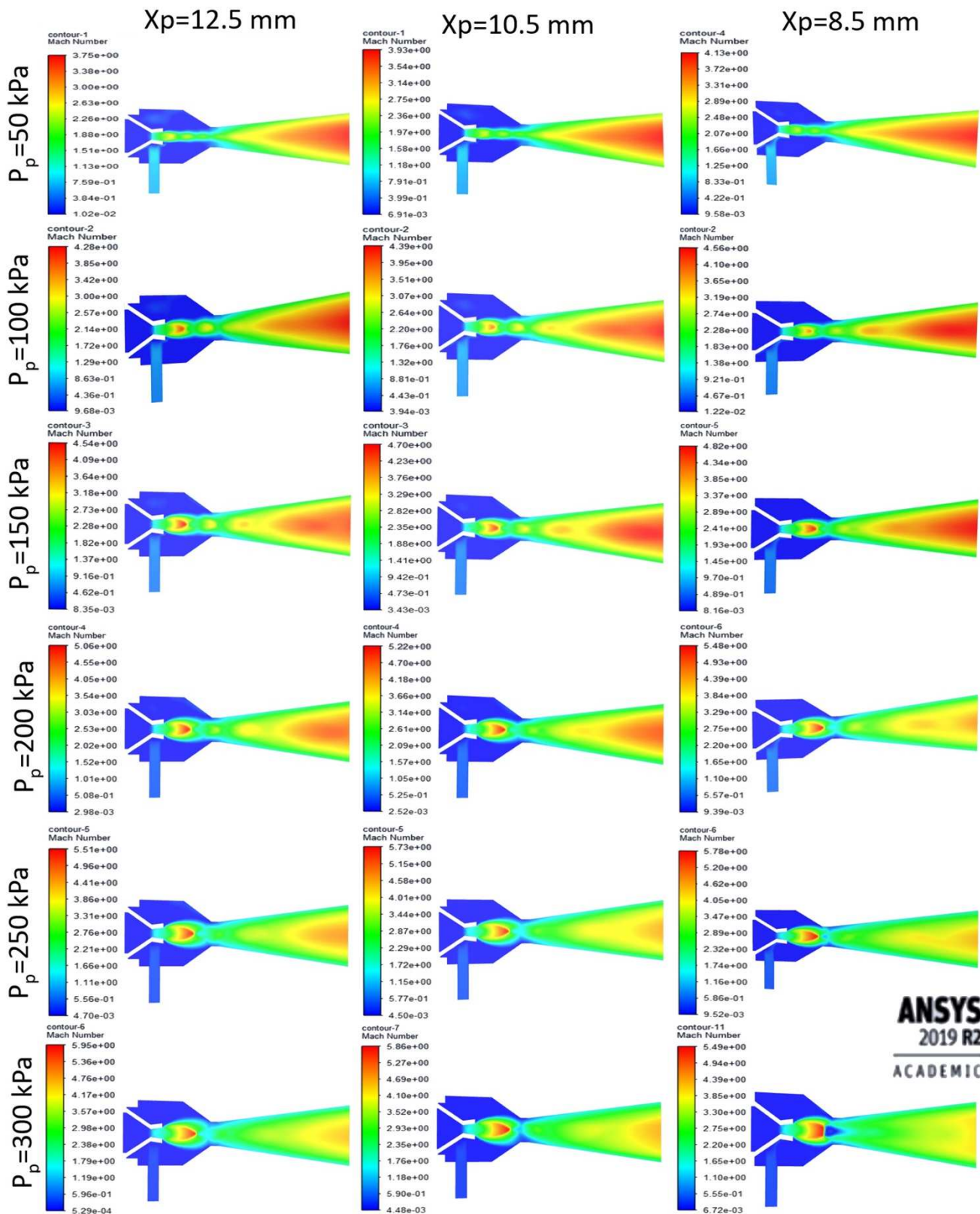


Fig. 10. Contours of Mach numbers for different inlet pressures and positions of primary nozzle.



The total pressure contours are represented in (Fig. 11). For all cases, the maximum pressures are given near the inlet of the primary fluid. For the first two inlet pressures considered, 50 kPa and 100 kPa, it can be seen that the distribution of the total pressure field does not considerably change with the position of the primary nozzle, X_p . For the remaining pressures, this observation is not applicable since the pressure distribution is significantly modified, especially between the outlet of the convergent-divergent nozzle and the outlet of the diffuser throat. As expected, in (Fig. 11), it can be observed that, for a particular position of the primary nozzle, X_p , the magnitude of the total pressure at each point of the fluid domain increases with the inlet pressure of primary fluid, P_p (with exception of the secondary fluid inlet where the pressure is kept at 8 kPa).

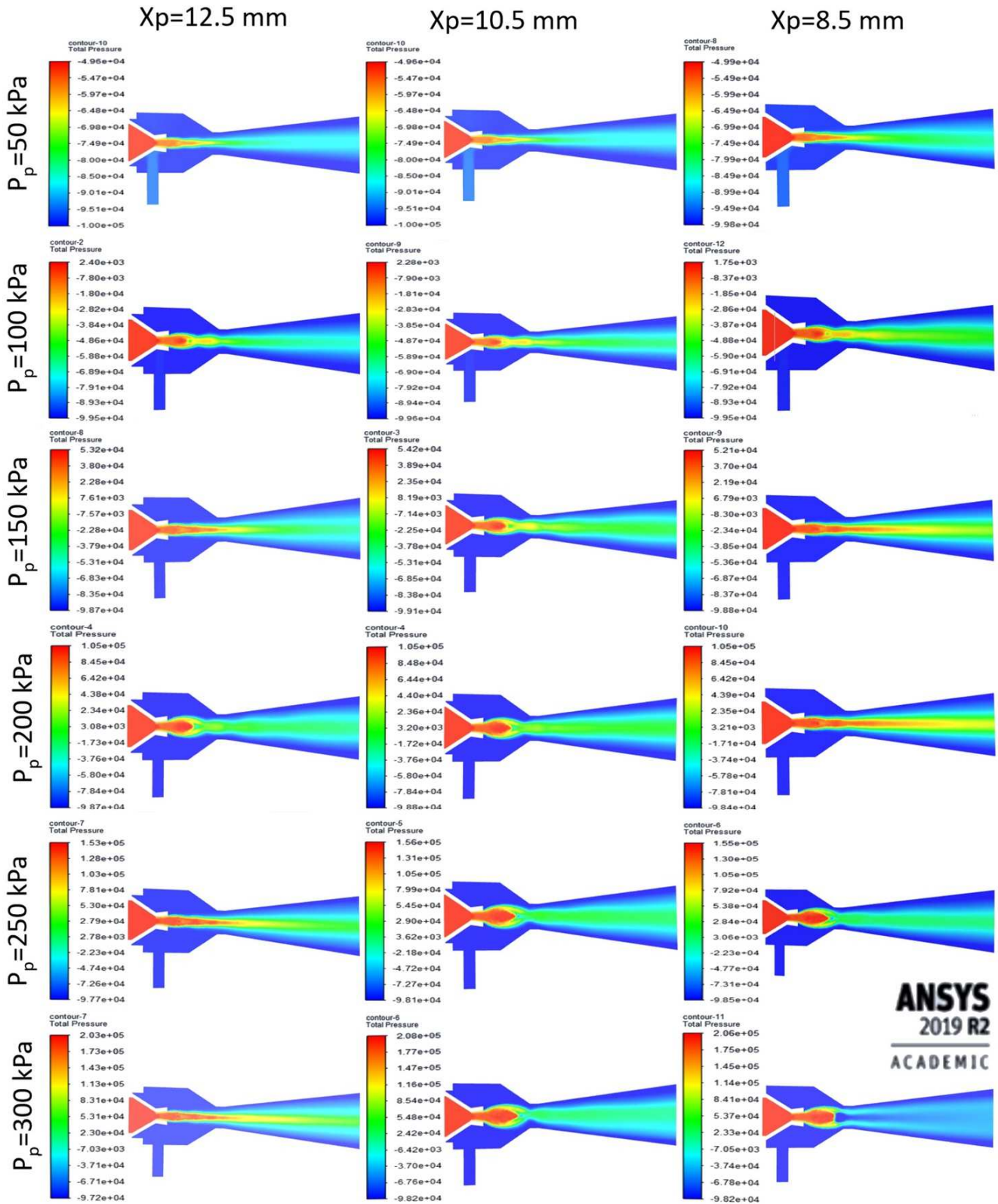


Fig. 11. Contours of pressure for different inlet pressures and positions of primary nozzle



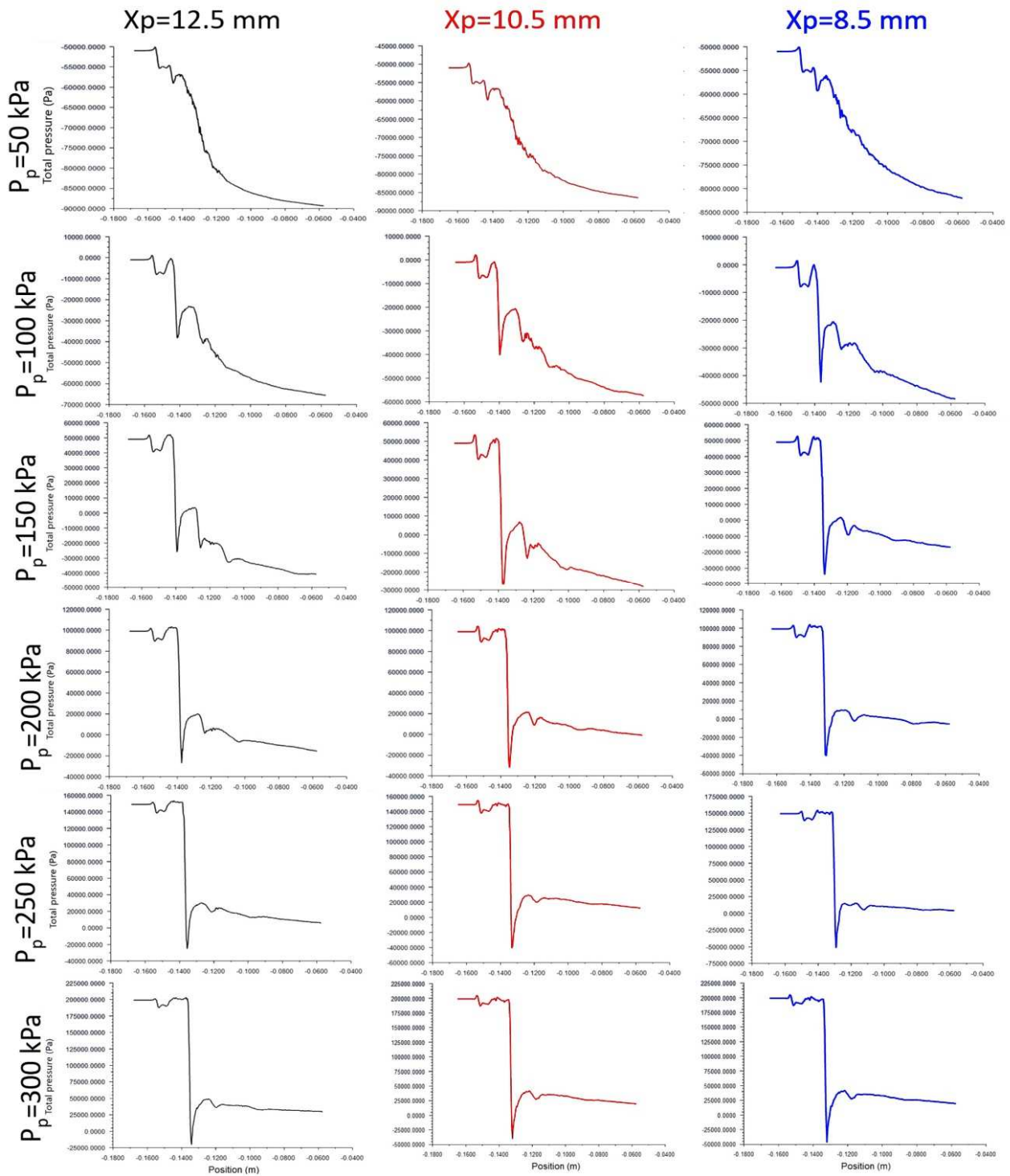


Fig. 12. Pressure profiles for different inlet pressures and positions of primary nozzle.

3.4 Influence of position and pressure of inlet nozzle on the longitudinal pressure profile.

In Fig. 12, the change of pressure along the midline of the symmetry plane is depicted for all cases considered in the present work. As can be observed, for inlet pressures of 50 kPa, 100 kPa and 150 kPa, minimum pressure is reached at the diffuser outlet, with exception of case corresponding to $X_p=8.5$ mm (primary nozzle closer to secondary one) and 150 kPa, where minimum pressure is obtained near the inlet of diffuser throat (where convergent section of suction chamber ends). For pressures greater than 150 kPa, minimum pressure takes place near the inlet of diffuser throat as well, corresponding with normal operating conditions of the jet pump. Under these normal conditions, it is worth noting that minimum pressure along the midline decreases as the primary nozzle is closer to the secondary one.

Outlet pressure of the diffuser is another important variable in the operation of the jet pump; in general, it must be lower than inlet pressure of primary fluid to avoid backflow towards the primary and secondary inlets. In the application considered in the present work (ethanol distillation), it is not necessary to obtain very high outlet pressures, oppositely to other cases, as fluid lifting. As expected, for a constant position of the primary nozzle (X_p), the larger the inlet pressure (P_p), the greater the outlet one (P_c); on the other hand, for a constant value of P_p , P_c increases as primary nozzle approaches to secondary one.



4. Conclusions

Computational fluid dynamics simulations of a jet pump for vacuum distillation of ethanol were carried out in the present work using standard $k-\epsilon$ turbulence model. Numerical results were compared with a previously developed unidirectional, analytical model to evaluate if this simple, low-cost model is able to reproduce similar results to the more realistic, time-demanding three-dimensional CFD simulations. Both approaches predict a similar general behavior of the fluid variables (pressure, velocity, Mach number) in the longitudinal direction of the jet pump when it operates in normal conditions, and analogous values of the inlet mass flow rate of primary fluid. However, significant differences between analytical and numerical results for some local variables (M_{e2} , M_4 , M_5 , P_5/P_4) were obtained. These differences are attributed mainly to the transverse variation of these variables, which can be significant according to numerical results; this is not captured in the analytical model.

On the other hand, CFD results were used to conduct a parametric analysis in terms of the inlet pressure, P_p , and position of the primary nozzle, X_p , and some general conclusions can be addressed from these results. Firstly, it is important to remind that the jet pump performance was quantified in the present work by three parameters: drag coefficient (w), Venturi effect as defined by the ratio between inlet and nozzle throat pressure (P_p/P_g), and the nozzle throat velocity (V_g). According to numerical results, for a constant value of X_p , the larger the inlet pressure, P_p , the lower the drag coefficient (w), the larger the Venturi effect (P_p/P_g) and the higher the nozzle throat velocity (V_g). This means that increasing the inlet pressure, P_p , does not necessarily improve all performance parameters of the jet pump, because even though P_p/P_g and V_g rises with P_p , the drag coefficient (w) decreases. A similar conclusion can be inferred for the position of primary nozzle, X_p , namely, a unique behavior of the pump performance, in terms of the three mentioned parameters, is not achieved. The closer the primary nozzle is to the secondary one, the larger V_g (increase of pump performance), but the lower the ratio P_p/P_g (decrease of pump performance), whereas the drag coefficient (w) is not considerably influenced by X_p .

Location of maximum and minimum Mach number and total pressure are important factors that account for the normal operation of the jet pump. In normal conditions, maximum Mach number of fluid domain is located between nozzle outlet and inlet of diffuser throat; according to CFD results, this condition is not reached for the two lower levels of inlet pressure considered here, i.e., $P_p=50$ kPa and $P_p=100$ KPa, where the Venturi effect, as defined by P_p/P_g , is very low, and jet pump operation can be considered abnormal. Additionally, the minimum total pressure does not take place at the suction chamber in these particular cases. The minimum Mach number and maximum total pressure near the inlet of primary fluid, which corresponds to normal operating pump conditions, are obtained in all CFD simulations. Additionally, numerical results showed that maximum Mach number and minimum total pressure has an increasing behavior with the inlet pressure of primary fluid, P_p . In normal operating pump conditions, the closer the primary nozzle is to secondary one, the lower the minimum total pressure; on the other hand, a unique behavior of the maximum Mach number with X_p was not obtained for all values of P_p .

Author Contributions

W.O. Murillo developed the mathematical modeling, examined the theory validation. J.A. Palacio-Fernandez planned the scheme and analyzed the empirical results. I.D. Patiño Arcila compared the results of the numerical simulation with those obtained by the analytical model. J.S. Zapata Monsalve developed the 3D CAD model of the jet pump. J.A. Hincapié Isaza loaded the parameters of the computational simulation into ANSYS Fluent™. The manuscript was written through the contribution of all authors. All authors discussed the results, reviewed and approved the final version of the manuscript.

Declaration of Competing Interest

We declare that we have no significant competing interests including financial or non-financial, professional, or personal interests interfering with the full and objective presentation of the work described in this manuscript.

Acknowledgement

The authors are gratefully acknowledged to the Institución Universitaria Pascual Bravo, Facultad de Ingeniería, Semillero de Investigación Ambiental (SIA), Grupo de Investigación e Innovación Ambiental (GIAM) and the Dirección de Tecnología e Innovación for their collaboration in the realization of this Project. We especially acknowledge to the industrial designer and teacher Nicolas Restrepo Henao of Institución Universitaria Pascual Bravo for their collaboration in graphics edition.

Nomenclature

A_2	Area at the exit of nozzle [m ²]	\dot{m}_p	Mass flow of primary fluid [kg/s]
A_4	Diffuser throat área [m ²]	M_{p2}	Mach number for isentropic air expansion at nozzle outlet.
A_g	Nozzle throat área [m ²]	M_{p2}^*	Critical Mach number of primary fluids at nozzle outlet.
A_p	Nozzle entry área [m ²]	P_2	Absolute pressure of primary fluid at nozzle outlet [kPa]
c	Velocity of sound at nozzle throat [m/s]	P_5	Mixing pressure at outlet of diffuser throat [kPa]
D_0	Diameter of Diffuser discharge [m]	P_c	Mixing pressure at diffuser outlet [kPa]
D_1	Diameter of nozzle inlet [m]	P_e	Absolute secondary fluid pressure [kPa]
D_2	Diameter of nozzle outlet [m]	P_p	Absolute air pressure at the nozzle inlet [kPa]
D_g	Diameter in the throat of the nozzle [m]	R	Gas constant [Nm/kgK]
D_p	Diameter of the suction chamber [m]	R_d	Length of divergent part of the diffuser [m]
D_t	Diffuser throat diameter [m]	S	Model sensitivity
k	Relationship of specific heats.	T_2	Primary fluid temperature at the nozzle outlet [K]
km	Relationship of specific heats of the mixture	T_e	Absolute temperature of secondary fluid [K]
K_S	Relationship of specific heats at secondary fluid	T_g	Primary fluid temperature at nozzle throat [K]



L	Straight part of the diffuser [m]	T_p	Air temperature at the nozzle inlet [K]
L_{1-g}	Length of nozzle inlet [m]	V_p	Primary fluid inlet velocity [m/s]
L_{g-2}	Nozzle discharge length [m]	w	Drag coefficient
M_4	Maximum Mach number at diffuser throat.	X	Distance from the nozzle discharge to diffuser throat [m]
M_4'	Critical Mach number at diffuser throat	α	Convergence angle of the diffuser [degrees]
M_5	Mach number at outlet of diffuser throat	β	Nozzle discharge angle [degrees]
M_{e2}	Mach number of secondary fluids at nozzle outlet	ρ_g	Density of primary fluid at nozzle throat [kg/m ³]
M_{e2}'	Critical Mach number of the secondary fluid at nozzle outlet.	ρ_p	Density of primary fluid at the nozzle inlet (Stagnation conditions) [kg/m ³]
\dot{m}_e	Mass flow of secondary fluid [kg/s]	θ	Angle of diffuser discharge [degrees]
\dot{m}_{max}	Maximum mass flow through the nozzle throat [kg/s]		

References

- [1] Besagni, G., Ejectors on the cutting edge: The past, the present and the perspective, *Energy*, 170, 2019, 998–1003.
- [2] Aidoun, Z., Ameur K., Falsafioon M, Badache M. Current Advances in Ejector Modeling, Experimentation and Applications for Refrigeration and Heat Pumps. Part 1: Single-Phase Ejectors, *Inventions*, 4, 2019, 2–73.
- [3] Tang, Y., Liu Z., Shi C., Li Y., A novel steam ejector with pressure regulation to optimize the entrained flow passage for performance improvement in MED-TVC desalination system, *Energy*, 158, 2018, 305–316.
- [4] Zheng, P., Li B., Qin J., CFD simulation of two-phase ejector performance influenced by different operation conditions, *Energy*, 155, 2018, 1129–1145.
- [5] Deng, X., Dong J., Wang Z., Tu J., Numerical analysis of an annular water–air jet pump with self-induced oscillation mixing chamber, *Journal of Computational Multiphase Flows*, 9, 2017, 47–53.
- [6] Varga, S., Oliveira A.C., Ma X., Omer S.A., Zhang W., Riffat S.B., Experimental and numerical analysis of a variable area ratio steam ejector, *International Journal of Refrigeration*, 34, 2011, 1668–1675.
- [7] Momeni, H., Domagała M. C.F.D. simulation of transport solid particles by jet pumps, *Czasopismo Techniczne*, 2M (7), 2016, 185–191.
- [8] Liu W., Pochiraju K., A methodology for the prediction of back-pressure induced stall in eductor-jet pumps, *International Journal of Refrigeration*, 95, 2018, 165–174.
- [9] Chandra, V. V., Ahmed MR., Experimental and computational studies on a steam jet refrigeration system with constant area and variable area ejectors, *Energy Conversion and Management*, 79, 2014, 377–386.
- [10] Arbab, A.B.A, Others, *Simulation of Ejector Flow Behavior Which Produce Vacuum in Power Plants Condenser*, MSc. Thesis, Sudan University of Science and Technology, Sudan, 2018.
- [11] Chen, J., Havtun H., Palm B., Investigation of ejectors in refrigeration system: Optimum performance evaluation and ejector area ratios perspectives, *Applied Thermal Engineering*, 64, 2014, 182–191.
- [12] Thongtip, T., Aphornratana S., An experimental analysis of the impact of primary nozzle geometries on the ejector performance used in R141b ejector refrigerator, *Applied Thermal Engineering*, 110, 2017, 89–101.
- [13] Chen, Z., Jin X., Dang C., Hihara E., Ejector performance analysis under overall operating conditions considering adjustable nozzle structure, *International Journal of Refrigeration*, 84, 2017, 274–286.
- [14] Fan, J., Eves J., Thompson H.M., Toropov VV, Kapur N, Copley D, et al. Computational fluid dynamic analysis and design optimization of jet pumps, *Computers and Fluids*, 46, 2011, 212–217.
- [15] Wang, X.-D., Dong J.-L., Numerical study on the performances of steam-jet vacuum pump at different operating conditions, *Vacuum*, 84, 2010, 1341–1346.
- [16] Yapici, R., Aldacs K., Optimization of water jet pumps using numerical simulation, *Proc Inst Mech Eng Part A J Power Energy*, 227, 2013, 438–449.
- [17] Aldas, K., Yapici R., Investigation of effects of scale and surface roughness on efficiency of water jet pumps using CFD, *Engineering Applications of Computational Fluid Mechanics*, 8, 2014, 14–25.
- [18] Shah, A., Chughtai IR, Inayat M.H., Experimental and numerical analysis of steam jet pump, *International Journal of Multiphase Flow*, 37, 2011, 1305–14.
- [19] Song, X-G., Park J-H, Kim S-G, Park Y-C., Performance comparison and erosion prediction of jet pumps by using a numerical method, *Mathematical and Computer Modelling*, 57, 2013, 245–53.
- [20] Dong, J., Wang X, Tu J., Numerical research about the internal flow of steam-jet vacuum pump: evaluation of turbulence models and determination of the shock-mixing layer, *Physics Procedia*, 32, 2012, 614–22.
- [21] Masud, J., Imran M., Turbulence Modeling for Realistic Computation of Internal Flow in Liquid Ejector Pumps, *54th AIAA Aerosp. Sci. Meet.*, Reston, Virginia: American Institute of Aeronautics and Astronautics, 2016.
- [22] Orozco, W., *Modelo matemático de una bomba chorro para la producción de 8 kPa que permita la destilación de etanol*, Instituto Tecnológico Metropolitano, Medellín, Colombia, MSc. Thesis, 2013.
- [23] Uyazán, AM, Gil ID, Aguilar JL, Rodríguez G, Caicedo LA., Deshidratación del etanol, *Ingeniería e Investigación*, 24, 2004, 49–59.
- [24] Orozco, W., Destilación al vacío de etanol usando bomba chorro, *Tecnológicas*, 25, 2010, 77–96.
- [25] Rusly, E., Aye L., Charters WWS, Ooi A. CFD analysis of ejector in a combined ejector cooling system, *International Journal of Refrigeration*, 28, 2005, 1092–1101.
- [26] Sriveerakul, T., Aphornratana S, Chunnanond K. Performance prediction of steam ejector using computational fluid dynamics: Part 1. Validation of the CFD result, *International Journal of Thermal Sciences*, 46, 2007, 812–822.
- [27] Huang, B.J., Chang J.M., Empirical correlation for ejector design, *International Journal of Refrigeration*, 22, 1999, 379–388.
- [28] Manrique, J. A., *Termodinámica*, Oxford University Press, Mexico, 2001.
- [29] El-Dessouky, H., Ettouney H., Alatiqi I., Al-Nuwaibit G., Evaluation of steam jet ejectors, *Chemical Engineering and Processing: Process Intensification*, 41, 2002, 551–561.
- [30] Robert, H., *Chemical engineer's hand book*, 7th ed, McGraw Hill, New York, 1997.
- [31] Sarkar, S., Lakshmanan B., Application of a Reynolds stress turbulence model to the compressible shear layer, *AIAA Journal*, 29, 1991, 743–749.
- [32] ANSYS Fluent 12.0 Theory Guide-4.4.2 RNG-Model 2009. <https://www.afs.enea.it/project/neptunius/docs/fluent/html/th/node59.htm>
- [33] ANSYS Fluent 12.0 User's Guide - 12.6.1 Setting up the Standard or Realizable - Model n.d.
- [34] Launder, B.E., Spalding, D.B., *Lectures in Mathematical Models of Turbulence*, Academic Press, London, 1972.
- [35] ANSYS Fluent 12.0 User's Guide - 26.13.1 Monitoring Residuals n.d. <https://www.afs.enea.it/project/neptunius/docs/fluent/html/ug/node812.htm>

ORCID iD

- William Orozco Murillo  <https://orcid.org/0000-0003-4115-0286>
 José Alfredo Palacio-Fernandez  <https://orcid.org/0000-0002-9207-7077>
 Iván David Patiño Arcila  <https://orcid.org/0000-0002-2876-8930>
 Johan Steven Zapata Monsalve  <https://orcid.org/0000-0001-5359-9051>
 John Alexander Hincapié Isaza  <https://orcid.org/0000-0002-6311-422X>





© 2020 by the authors. Licensee SCU, Ahvaz, Iran. This article is an open access article distributed under the terms and conditions of the Creative Commons Attribution-NonCommercial 4.0 International (CC BY-NC 4.0 license) (<http://creativecommons.org/licenses/by-nc/4.0/>).

How to cite this article: Murillo W.O., Palacio-Fernandez J.A., Patiño Arcila I.D., Zapata Monsalve J.S., Hincapié Isaza J.A. Analysis of a Jet Pump Performance under Different Primary Nozzle Positions and Inlet Pressures using two Approaches: One Dimensional Analytical Model and Three Dimensional CFD Simulations , *J. Appl. Comput. Mech.*, 6(SI), 2020, 1228–1244. <https://doi.org/10.22055/JACM.2020.33339.2205>

